

Mass growth and density profiles of dark matter halos in hierarchical clustering

Adi Nusser & Ravi K. Sheth

Max-Planck Institute für Astrophysik

Karl-Schwarzschild-Str. 1

85740 Garching, Germany

22 June 2021

ABSTRACT

We develop a model for the growth of dark matter halos and use it to study their evolved density profiles. In this model, halos are spherical and form by quiescent accretion of matter in clumps, called satellites. The halo mass as a function of redshift is given by the mass of the most massive progenitor, and is determined from Monte-Carlo realizations of the merger-history tree. Inside the halo, satellites move under the action of the gravitational force of the halo and a dynamical friction drag force. The associated equation of motion is solved numerically. The energy lost to dynamical friction is transferred to the halo in the form of kinetic energy. As they sink into the halo, satellites continually lose matter as a result of tidal stripping. The stripped matter moves inside the halo free of dynamical friction. The evolved density profiles are steeper than those obtained by assuming that, once they have been accreted onto the parent halo, satellites remain at a fixed distance from the halo center. We find that the final density profile depends mainly on the rate of infall of matter onto the halo. This, in turn, depends on the initial fluctuation field as well as on cosmology. For mass scales where the effective spectral index of the initial density field is less than -1 , the model predicts a profile which can only approximately be matched by the one parameter family of curves suggested by Navarro, Frenk and White (1997). For scale-free power-spectra with initial slope n , the density profile within about 1% of the virial radius is $\rho \propto r^{-\beta}$, with $3(3+n)/(5+n) \leq \beta \leq 3(3+n)/(4+n)$.

Key words: cosmology: dark matter-galaxy formation

1 INTRODUCTION

A long standing question in the dynamics of cosmological gravitating systems is: how well do dynamically evolved systems retain memory of their initial conditions? On large scales, where the evolution is still in the the weakly non-linear regime, the growing mode of the initial density fluctuations can, in principle, be fully recovered, if the present velocity or density field is given (*e.g.*, Peebles 1989, Nusser & Dekel 1992). On small scales where shell crossing has occurred and “virialised” objects (halos) have formed, the situation is less clear. Using techniques of statistical mechanics, Lynden-Bell (1967) showed that starting from a general initial state, a gravitating system could, via a process he termed “violent relaxation”, reach a quasi-equilibrium state which is almost independent of the initial conditions. Therefore, under the restricted conditions he assumed in his analysis, a gravitating system develops a “universal” density profile independent of the initial conditions.

The assumptions underlying Lynden-Bell’s analysis are hard to justify in the hierarchical scenario for the formation of structure in an expanding universe. Nevertheless, high resolution cosmological N-body simulations of the gravitational clustering of collisionless particles from hierarchical initial conditions strongly suggest that dark matter halos do indeed develop a universal final density profile (*e.g.* Dubinski & Calberg 1991, Lemson 1995, Navarro Frenk & White 1995, 1996, Cole & Lacey 1996, Moore et. al. 1997). Navarro, Frenk & White (1995, 1996; hereafter NFW) found that density profiles of halos of different masses in a variety of cosmological models could be fit with the following one parameter functional fit

$$\frac{\rho_N(r)}{\rho_b} = \frac{\delta_N}{\frac{r}{r_v} \left[1 + c \frac{r}{r_v}\right]^2}, \quad (1)$$

where ρ_b is the background density and r_v is the virial radius of the halo, defined as the radius within which the average density is 178 times that of the background. With this definition for r_v , the parameter δ_N can be expressed in terms of the concentration parameter c ; thus, c is the only free parameter in the fit (1). It has been argued by NFW that c is directly related to the formation time of a given halo. The claim that density profiles could be fitted with a one parameter functional form, has recently been challenged by Klypin et. al. (1998) who found, using N-body simulations of CDM-like models, that the scatter about a one parameter fit is substantial, indicating that the structure of halo density profiles involves more than just one physical parameter.

Because of the lack of a general analytic technique for following the detailed evolution of a system from general initial conditions, most analytic work has focused on studying the evolution of isolated spherical systems (Gunn & Gott 1972). The collapse of a spherical density perturbation of a self-similar form, $\delta \propto r^{-m}$, in an otherwise flat universe, yields the density profile $\rho \propto r^{-3m/(1+m)}$ for $m \geq 2$, and $\rho \propto r^{-2}$ for $m < 2$ (Filmore & Goldreich 1984, Bertschinger 1985). This implies that in highly non-linear systems, full information about the initial distribution is preserved only for a special class of initial conditions. Strictly speaking, this result is valid only for the case of purely radial collapse. In principle, non-radial motions can prevent particles with large turnaround radii from sinking to the inner regions of the collapse and forming an r^{-2} profile. If particles were assigned angular momenta in a self-similar way, then the density profile above is expected to be valid when $m < 2$ as well (White & Zaritsky 1992).

These special spherical solutions were first related to the formation of dark matter halos from initial gaussian density fields by Hoffman & Shaham (1985) (also see Hoffman 1988). They noted that the mean shape of high peaks in gaussian fields is $\delta \propto r^{-(n+3)}$ where n is the index of the initial power spectrum (Dekel 1981, Bardeen et al. 1986). Therefore, they argued that setting $m = n + 3$ makes the spherical solutions relevant in the cosmological context. There are two caveats to this argument. First, it assumes that the accreting matter is not clumpy. In contrast, in hierarchical scenarios for structure formation, halos grow in mass by mergers with other, typically less massive, halos (cf. Lacey & Cole 1994; Lemson 1995; Syer & White 1996). This means that the effects of dynamical friction and tidal stripping may well be important in determining the final structures of halos in hierarchical models. Second, one is usually interested in the density profiles of halos of a given mass today; these may have had, as their seeds, initial density peaks of various heights and shapes. Moreover, strictly speaking, the Hoffman & Shaham (1985) solution applies only in regions outside the virial radius of a dark matter halo. In fact, Syer & White (1996) argue that the profile must scale as $r^{-\beta_{\text{SW}}}$ with $\beta_{\text{SW}} = 3m/(2 + m)$ in the inner regions of dark matter halos, and this solution differs from the $r^{-\beta_{\text{HS}}}$, with $\beta_{\text{HS}} = -3m/(1 + m)$, scaling proposed by Hoffmann & Shaham (1985).

Since understanding the density profiles of halos is necessary to relate structure formation theory to the observed structure of galaxies, we aim here to develop a more detailed model of the process of halo formation. We will continue to assume spherical symmetry, and will formulate a semi-analytic scheme for modelling the evolution and the structure of halos more realistically. The first goal of this paper is to develop and test a method for tracing the mass of a given halo back in time that is consistent with the hierarchical clustering scenario. We describe this method briefly in section 2.1 (details are discussed in the Appendix). Our second goal is to provide a simple model, which includes the effects of dynamical friction and tidal stripping, for the motion of satellites once they are inside a halo, and to then use this model to estimate the halo structure that results. In section 2.2 we describe how to treat the motion of satellites once they are inside the halo. The equation of motion must be solved numerically and, in section 3, we present the results of applying this scheme to simulate the evolution of a variety of halos. We study halos of various masses that form from initially scale free gaussian fluctuation fields as well as fields with the CDM power spectrum. In section 4 we conclude with a discussion of our results and argue that the concentration scale c in the NFW profile, if fundamental, cannot directly be related to the formation time and must reflect an interplay between the formation time and other—yet unknown—physical effects, which determine the halo profile.

2 THE MODEL

We will compute the evolved density profile of a halo which has mass M_0 at the final redshift z_0 in two steps. First, we devise a scheme for tracing back, to some early time, the mass of the largest progenitor subclump of the halo. The rate of change of the mass of the most massive progenitor (MMP) gives the accretion rate of matter onto the already existing halo. This rate is sensitive to the background cosmology, and to the shape of the initial power spectrum. Our second step is to formulate a dynamical prescription for following the evolution of the accreted matter inside the halo.

2.1 Halo Mass Growth Rate

At any given redshift z , define the current virial radius, r_v , of a halo as the radius within which the average density is $178\rho_b$, where ρ_b is the mean density in the universe at that time. At z , the current halo mass is defined as the mass within the current virial radius. Ofcourse, the current virial radius and mass are smaller than their final values. Two key ingredients in our model are (i) how the mass within the virial radius grows with time, and (ii) how the accreting mass is distributed among satellites. To provide these two ingredients, one must trace the full merger history of a given halo back in time. That is, we need to know how the mass M_0 was partitioned into progenitor halos at any earlier time $z_1 > z_0$. For Gaussian initial conditions, merger history trees of halos, each of which has the same mass M_0 at z_0 , can differ substantially. Therefore, we need to list all possible merger trees, and we need to compute the probability that each occurs. Except for Poisson initial conditions (Sheth 1996), this probability has not been computed analytically. Hence, we adopt a short-cut. We trace only the most massive progenitor of the most massive progenitor, and so on, back in time.

We do this as follows. We assume that at z_1 , the average number of progenitors of an (M_0, z_0) -halo that have mass between M_1 and $(M_1 + dM_1)$ can be approximated by

$$\begin{aligned} N(M_1, z_1|M_0, z_0) dM_1 &= \left(\frac{M_0}{M_1}\right) \frac{1}{\sqrt{2\pi}} \frac{\delta_c(z_1 - z_0)}{(S_1 - S_0)^{3/2}} \exp\left[-\frac{\delta_c^2(z_1 - z_0)^2}{2(S_1 - S_0)}\right] \left|\frac{dS_1}{dM_1}\right| dM_1 \\ &\equiv \left(\frac{M_0}{M_1}\right) f(M_1, z_1|M_0, z_0) dM_1 \end{aligned} \quad (2)$$

(Bower 1991, Lacey & Cole 1993), where $\sqrt{S_i}$ is the *rms* density fluctuation in a Top-Hat window function of radius $(3M_i/4\pi)^{1/3}$. Lacey & Cole (1994) show that this expression is in good agreement with what happens in numerical simulations (but see Tormen 1998). The second equality defines $f(1|0)$, which is the fraction of the mass of M_0 that, at z_1 , was in objects with mass M_1 . This means, of course, that the integral of $f(1|0)$ over the range $0 \leq M_1 \leq M_0$ equals unity. However, as $(z_1 - z_0) \rightarrow 0$, the integral of $N(M_1, z_1|M_0, z_0)$ over the range $(M_0/2)$ to M_0 also approaches unity. Since an M_0 halo may have at most one progenitor with mass in this range, $N(1|0)$ can be interpreted as the probability that an (M_0, z_0) -halo had an (M_1, z_1) progenitor subhalo (cf. Lacey & Cole 1993), with (M_1/M_0) restricted to the range between one half and unity, a short time earlier. Consequently, in the limit of small redshift intervals, we choose the mass of the MMP according to equation (2). We then replace M_0 with the chosen value of M_1 , and z_0 with $z_1 > z_0$, and iterate until M_1 , the mass of the MMP is as small as desired. In the Appendix we argue that this scheme provides MMP histories that are similar to those which occur in numerical simulations.

In what follows, the ensemble average of the accretion rate will be useful. Before computing it, the following question arises: should we use curves of $M(z)$ by averaging the masses of all realisations of merger histories in the mass direction given the redshift, or should we use $M(z)$ obtained by averaging the redshift at a given mass? Fortunately, the two ways of averaging lead to almost identical curves of $M(z)$. Figure 1 shows curves of $M(z)$ for halos having $M_0/M_* = 1, 3$ and 10 , for scale free power spectra with $n = 0, -1$ and -2 . Also shown are results for halos having $M = 10^{11}, 10^{13}$ and $10^{15} M_\odot$ in the standard CDM model, normalised such that the linear *rms* value of density fluctuations in a spherical window of radius $8h^{-1}\text{Mpc}$ is $\sigma_8 = 0.6$. The solid lines show curves obtained by averaging the mass at a given redshift, and the dashed lines show curves obtained by averaging the redshift at a given mass. The error bars are $1\text{-}\sigma$ deviations from the mean $M(z)$. The dashed and the solid lines corresponding to each case almost overlap. This figure also shows the well known fact that, on average, lower mass halos formed at an earlier epoch. In what follows we have arbitrarily chosen to work with $M(z)$ obtained by averaging the merger histories in the mass direction. *

2.2 Density profiles from stable clustering

One way to convert the mass growth curves $M(z)$ to density profiles is as follows. We assume that the mass $M(z - dz) - M(z)$ accreted during dz is accreted smoothly onto the MMP. This means that we are ignoring the fact that this mass may actually be divided among subclumps. Assume that a newly accreted patch of matter oscillates around the center of the halo with mean radius equal to the virial radius of the halo at the redshift at which it joined the halo. This is the *stable clustering* assumption, since it is equivalent to assuming that there is no net in-flow of matter in the virialised region. It is motivated by

* When the mass of the MMP is greater than half of M_0 , then $M(z)$ can be computed directly from the formation time argument given in the Appendix. The mean value of the scaled variable there, ω_f , is

$$\int_0^\infty \omega_f p(\omega_f) d\omega_f = \sqrt{\frac{2}{\pi}} \left(\frac{2}{3} + \frac{1}{3f}\right), \quad (n = 0)$$

from which the mean value of z given $M(z)/M_0$ is easily obtained.

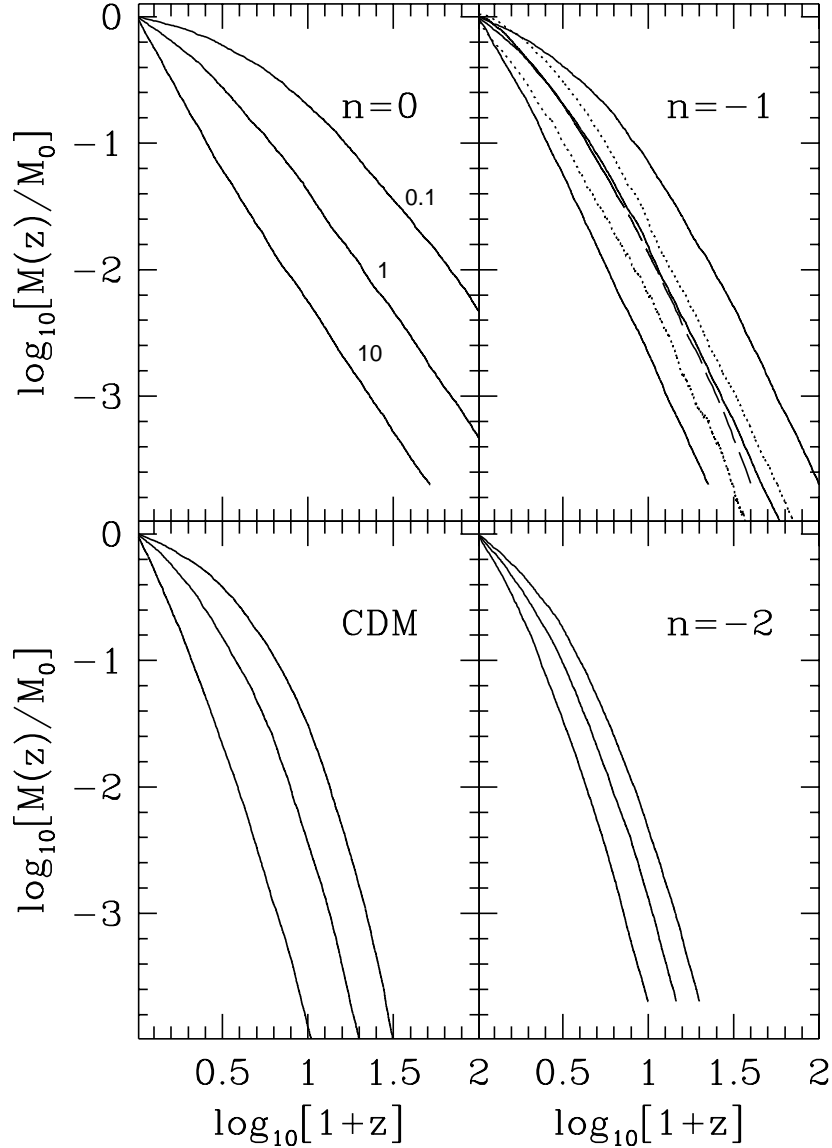


Figure 1. Curves of the average $M(z)/M_0$ for power law spectra with $n = -2, -1$ and 0 , as indicated in the plot. The solid curves, in each panel, correspond, from top to bottom, to $M/M_* = 0.1, 1$ and 10 obtained by averaging in the mass direction. The dotted lines in the middle panel lines are 1σ deviations about the mean $M(z)$ for $1M_*$ halo. The dashed line in the middle panel is $M(z)$ for $1M_*$ obtained by averaging in the redshift direction.

the analytic solutions for collapse of density peaks with pure power law initial profiles (Filmore & Goldreich 1984; Bertschinger 1985). Recall that, in these solutions, the mean density within a radius r of the halo is a multiple (here we use 178) of the background density of the universe at the time when the virial radius of the halo was r . Indeed, in this approximation, our only change to the Hoffman & Shaham (1985) study is our method for computing the accretion rate. A similar analysis was also done by Avila-Reese, Firmani & Hernández (1997) who used the prescription of Lacey & Cole (1993) and Eisenstein & Loeb (1996) to compute $M(z)$.

Ideally, one would like to use stable clustering to compute final profiles for each individual merger history and then average the result over many realisations. In practice this is time consuming. We show below (Figure 4) that the evolved

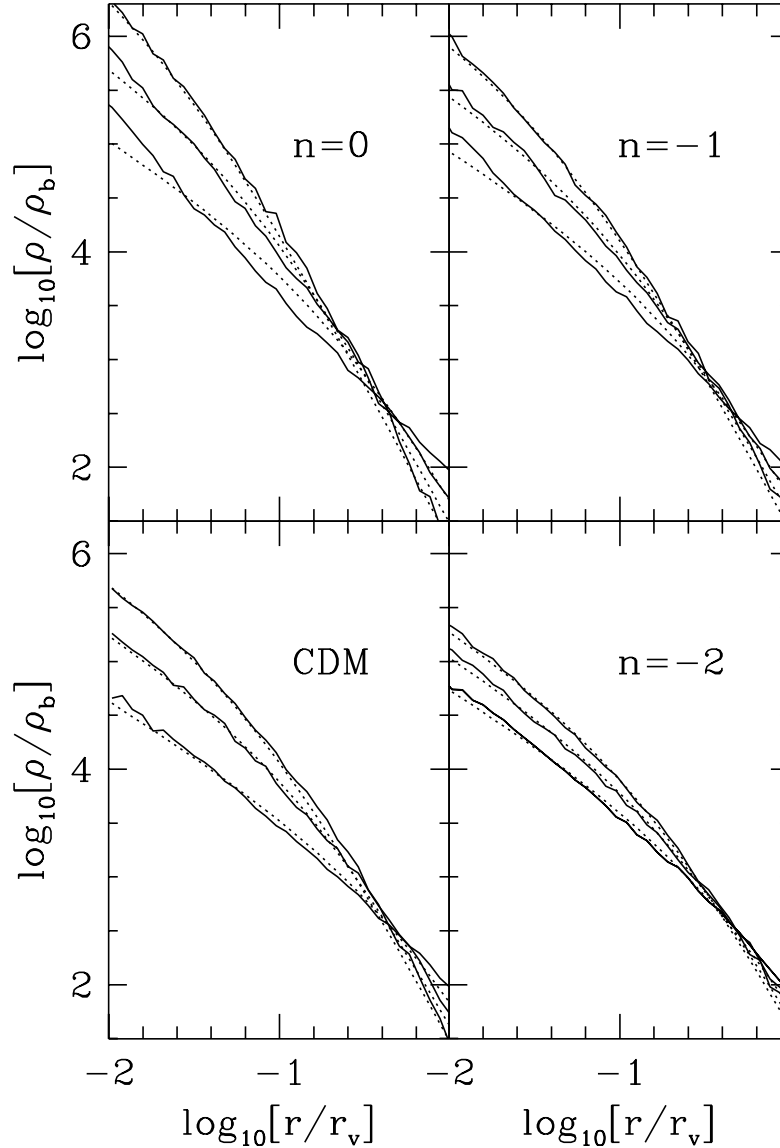


Figure 2. Density profiles obtained from curves of $M(z)$ under the assumption of stable clustering. The dotted curves are the NFW best fits to the density profiles.

density profile computed from the ensemble averaged $M(z)$ is a good approximation to the ensemble average of the individual evolved profiles. To do so, we have used the stable clustering assumption to compute profiles of 10 random realisations of the merger tree of an M_* halo for a scale free spectrum with $n = -1$. The average of these profiles is the dashed curve in figure 4. The profiles from six individual merger histories are shown by the light solid curves. The thick solid line is the profile obtained from the average $M(z)$ shown in figure 1. We conclude from figure 4 that, at least under the assumption of stable clustering, working with the average $M(z)$ does not introduce systematic biases.

The density profiles generated in this way from the ensemble averaged $M(z)$ curves of Fig. 1 are shown in Fig. 2. The dotted lines are fits of the form NFW form given in (1). Figure 3 shows the associated circular velocity profiles: $V_c^2(r) \propto GM(r)/r$. Except when $n = 0$, the individual density and circular velocity profiles are reasonably well described by the NFW parametric

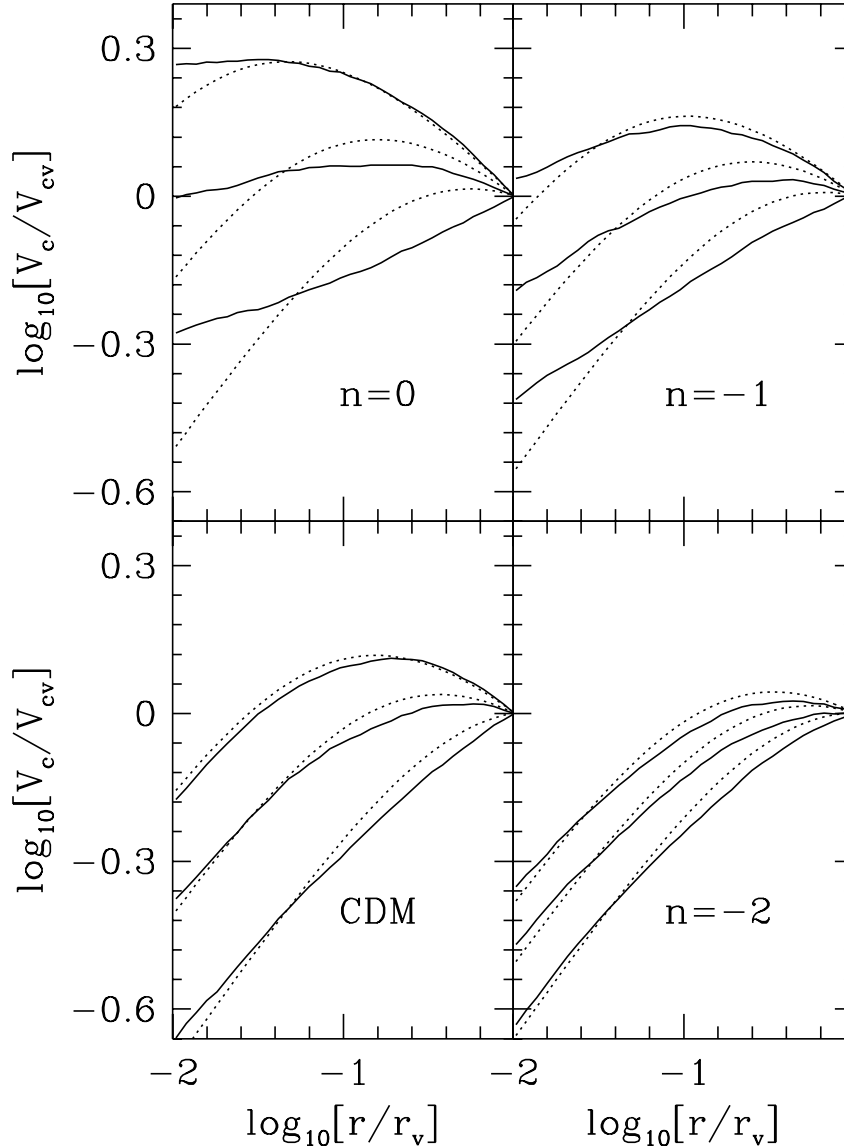


Figure 3. The same as the previous figure but showing rotation curves instead of density profiles.

form. Notice that less massive halos are more centrally concentrated. The trend of steeper profiles for larger values of the spectral index, n , is also seen in the simulations (e.g. Cole & Lacey 1996). There is, however, a fundamental difference between the profiles obtained here and those in the simulations. For example, in the CDM N-body simulations, profiles of halos with masses $\sim 10^{11} M_{\odot} - \sim 10^{15} M_{\odot}$ almost coincide over the range $0.1 > r/r_v < 1$ (cf. figure 4 in NFW 1995). On the other hand, the corresponding profiles in figure 2 substantially deviate from each other for the same range. Thus, the concentration parameter c depends differently on mass in our models than it does in the simulations. NFW argue that c is determined by the formation time of halos. Our detailed models of the accretion history incorporate this formation time explicitly, yet, they are unable to reproduce the trends of c with mass that are seen in simulations. This suggests that, if simulated halos are indeed well described by the one parameter c , then this parameter must depend on more than just the formation time; c must depend on some additional physics.

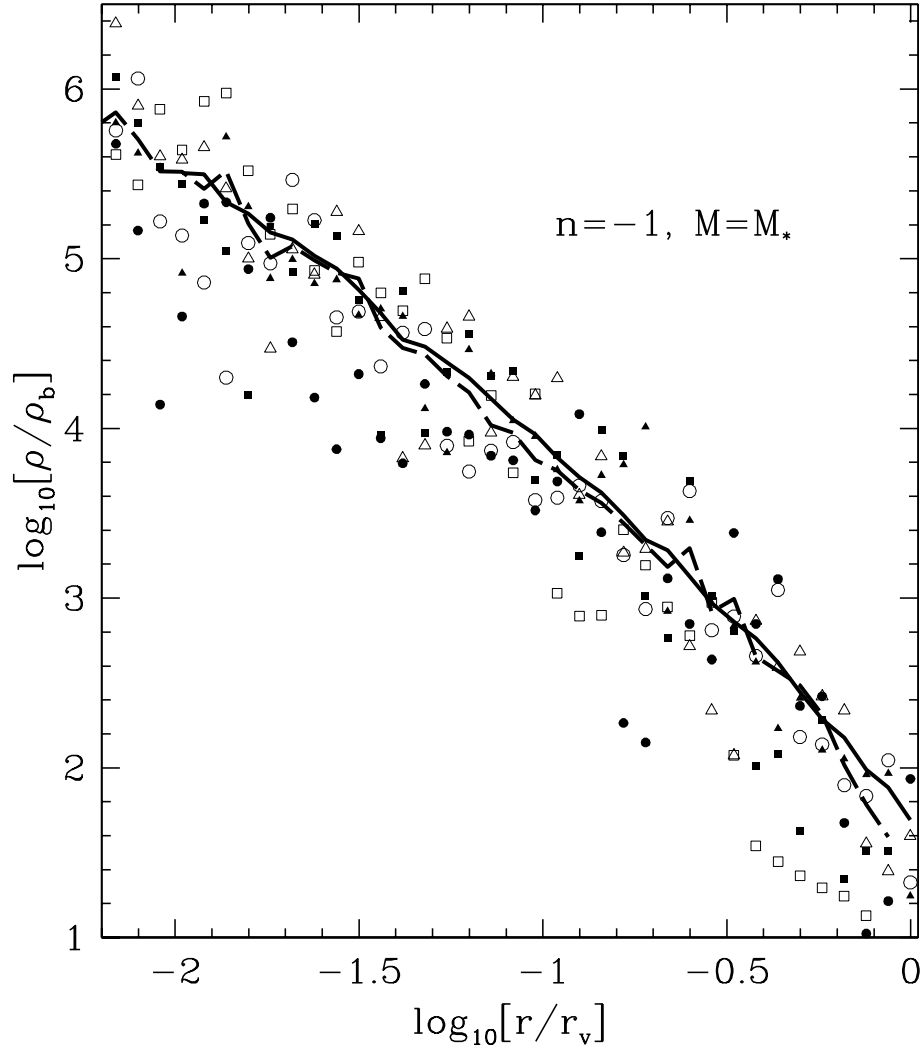


Figure 4. Density profiles from 6 random realisations (points) of $M(z)$ for $n = -1$ and $1M_*$ halo. Plotted also is the average profile (heavy dashed) of 10 random realisations and the profile (heavy solid) corresponding to the average $M(z)$. The profiles were computed under the stable clustering assumption.

The stable clustering assumption is not expected to hold in realistic collapse configurations. This is because the accreting matter is, in fact, distributed into bound clumps (satellites). These will suffer from dynamical friction as they fall into the halo. This causes a transfer of energy from the satellites to the halo which is neglected in the stable clustering collapse considered above. Moreover, the tidal field of the halo continuously prunes infalling satellites, and this is also ignored in the smooth collapse scenario. In the next section we describe how to compute evolved density profiles which include these effects.

2.3 Beyond stable clustering: dynamical friction, tidal stripping and halo heating

In this section we formulate a dynamical model of the motion of satellites inside halos. The treatment here does not require any assumptions about the matter accretion rate, provided major mergers do not occur. Indeed mergers of two halos of similar mass invalidate the dynamical prescription presented here.

We will write the equations of motion of satellites inside a halo under the approximation that the halo is spherical. Then, the gravitational field of the halo is that of a spherical mass distribution. In addition to the gravitational field of the halo, satellites suffer from a dynamical friction drag force (Chandrasekhar 1943). Therefore, the equations governing the motion of a satellite within a halo are,

$$\frac{d^2\mathbf{r}}{dt^2} = -\omega_{\text{df}}(r, t) \frac{d\mathbf{r}}{dt} - M_{\text{h}}(r, t) \frac{\mathbf{r}}{r^3}, \quad (3)$$

where $M_{\text{h}}(r, t)$ is the mass of the halo within radius r at time t and ω_{df} is the inverse of the dynamical friction time.[†] Ostriker & Turner (1979) derived a similar expression. For a satellite of mass M_{s} moving in a medium of density, ρ , and velocity dispersion, σ , the quantity ω_{df} , can be approximated by

$$\omega_{\text{df}}(r, t) = \mathcal{N} M_{\text{s}} \frac{\rho(r, t)}{\sigma^3(r, t)} \quad (4)$$

(Binney & Tremaine 1987), where \mathcal{N} is a numerical factor. Here $\sigma(r, t)$ and $\rho(r, t)$ represent the average velocity dispersion and density within r .

The gravitational field of the halo prunes the satellites as they sink to the center of the halo. This causes a gradual decrease in the mass of the satellite, M_{s} , which should be taken into account in the equations of motion (3). We assume that a satellite at a distance r from the center of the halo retains only matter which lies inside a certain radius, the tidal radius r_{t} , from its center. This tidal radius is approximately that radius at which the gravitational field of the satellite equals the change in the gravitational field of the main halo times r_{t} . That is,

$$\frac{\partial}{\partial r} \left(\frac{M_{\text{h}}}{r^2} \right) r_{\text{t}} = \frac{M_{\text{s}}}{r_{\text{t}}^2}, \quad (5)$$

which, to first order in r_{t}/r , reduces to

$$\frac{M_{\text{s}}(r_{\text{t}})}{r_{\text{t}}^3} = \frac{M_{\text{h}}(r)}{r^3}. \quad (6)$$

Thus, the average density of the satellite within r_{t} equals the average density of the halo within r . Given a guess about the density profile of the satellite when it crosses the virial radius of the halo, and assuming that the profile within r_{t} does not change with time, the relation (6) determines the mass of the satellite as a function of r .

Here we assume that satellites are spherical and have $1/r^2$ density profiles, i.e., $M_{\text{s}}(r_{\text{t}}) \propto r_{\text{t}}$. In this case, as a satellite of mass M_{sv} passes through a halo of density ρ_{v} , it loses mass according to

$$M_{\text{s}}(r) = \left(\frac{\rho_{\text{v}}}{\rho_{\text{h}}(r)} \right)^{1/2} M_{\text{sv}}, \quad (7)$$

where $M_{\text{s}}(r)$ is the mass of the satellites mass when it is at radius r and $\rho_{\text{h}}(r)$ is the average density of the halo within that radius. Substituting this in (4), and using the fact that $M_{\text{h}}(r)/r \propto \sigma^2(r)$, we find that

$$\omega_{\text{df}} = \alpha \left(\frac{\rho_{\text{v}}}{3\pi} \right)^{1/2} \frac{M_{\text{hv}}}{M_{\text{h}}(r)}, \quad (8)$$

where $\alpha = \sqrt{3\pi} \mathcal{N} M_{\text{sv}}/M_{\text{hv}}$, and M_{hv} is the mass of the halo when the satellite crossed its virial radius. The factor α is scaled so that it is the ratio of the circular orbit time to the dynamical friction time at the time when the satellite joined the halo.

Matter stripped from satellites is said to be ‘evaporated’. Initially, evaporated matter is assigned the velocity and position of the satellite from which it was stripped. Thereafter, it moves under the influence of the gravitational field of the halo free of dynamical friction. Of course, the satellite, now with reduced mass, continues to suffer from dynamical friction.

Next, we need to determine the fate of the energy that is lost by satellites as a result of the dynamical friction term in the equation of motion (3). A satellite loses energy at the rate

$$\frac{d(E/M_{\text{s}})}{dt} = -\omega_{\text{df}} \left(\frac{d\mathbf{r}}{dt} \right)^2 \quad (9)$$

[†] We work in units in which $G = 1$.

(cf. Landau & Lifshitz 1960). It is unclear how this lost energy is redistributed within the halo. Since the bulk of the halo's matter contributes to the dynamical friction drag force which is exerted on the satellites, it seems reasonable to assume that the lost energy is distributed equally among the halo matter. That is, the energy deposited to a patch of evaporated matter is assumed to be proportional to its mass.

2.3.1 Numerical Scheme

The equations of motion above can be solved numerically, provided that we make a number of additional assumptions which we describe below.

Our numerical scheme simulates a halo made of particles of identical mass. Some of these particles are assigned to satellites and suffer from dynamical friction; the other particles move under the influence of the gravitational field of the halo only and are called halo particles. The code treats these two types of particles differently. Since a satellite particle may be tidally stripped from its parent, we need some way of deciding when this happens; once stripped the particle becomes a halo particle, and can never be captured by satellites. Dynamical friction provides a mechanism for the transfer of energy from satellites to the halo; the code allows for this by assuming that only halo particles can absorb this energy. We describe how both these effects are included in more detail below.

We follow the evolution of a halo starting at an early time at which the halo mass was a tiny fraction of its final mass. Given the growth of the mass of the halo with time, we can compute the time at which each particle will cross the virial radius of the halo. At any given time, we simulate only the trajectories of those particles which are within the current virial radius. We assume that, when first accreted, particles move on circular orbits.

Since we are only simulating particles within the current virial radius, some of these particles may have already been stripped from their parent satellites. Here we assume that about half the particles joining the halo in any given time step are associated with satellites and the other half are halo particles. We need to specify the parameter α for all those particles which belong to satellites. Notice that equations (3) and (8) involve the mass of a satellite only through the parameter α which determines the dynamical friction time scale. This simplifies the problem considerably. In the numerical scheme, each satellite's particle is assigned a value of α drawn from a uniform distribution with a minimum value of zero and some maximum value, α_{\max} , which determines the total energy lost by the satellites.

This choice implies that, at any time, the average satellite mass is proportional to the mass of the MMP. This is in the spirit of hierarchical clustering and is motivated by results from N-body simulations (Tormen 1997). Now we need to decide which particles are stripped, and when. At any given time, each satellite particle is assigned a probability of remaining bound to its parent. According to equation (7) this probability is proportional to the ratio of the average density within the particle's radius at the current, to that at the previous time step.

Finally, in order to avoid numerical instabilities, the gravitational force acting on a particle at radius r_i is softened according to

$$\mathbf{F}_{gi} = -\frac{mN_i\mathbf{r}_i}{(r_i^2 + \epsilon^2)^{3/2}} \quad (10)$$

where m is the particle's mass, N_i is the number of particles with $r < r_i$ and ϵ is the force softening parameter. For a closed system of particles without dynamical friction this force law conserves the total "energy"

$$E_{tot} = m \sum_i \left[\frac{\dot{\mathbf{r}}_i^2}{2} - \frac{mN_i}{(r_i^2 + \epsilon^2)^{1/2}} \right] \quad (11)$$

(White 1983). The factor ω_{df} , which determines the amplitude of the dynamical friction drag force, is evaluated according to

$$\omega_{df\ i} = \alpha_i \rho_{vi}^{1/2} \frac{M_{hvi}}{mN_i}, \quad (12)$$

where M_{hvi} and ρ_{vi} are the mass and the average density of the halo within the virial radius at the time the satellite was accreted onto the halo. The sorting routine INDEXX in Press et. al. (1992) reduces the evaluation of the gravitational and dynamical friction forces to an $N \log_2 N$ process, where N is the total number of particles in the halo at any given time step. Once the forces have been computed, a leapfrog time integration scheme is used to move particles from the current time step to the next. In each time step the energy lost by satellite particles is computed using (9). The satellites lost energy is distributed equally among the halo particles in the form of kinetic energy. Namely, halo particles absorb the energy lost by satellites by receiving "kicks" in random directions.

Increasing α_{\max} increases the total amount of energy lost by the satellites. Unfortunately, the code is unstable for values of α_{\max} which lead to energy loss exceeding a significant fraction of the absolute value of the total energy. We will see that even a small amount of heating is sufficient to significantly change the halo density profile in the inner region relative to the stable clustering profiles.

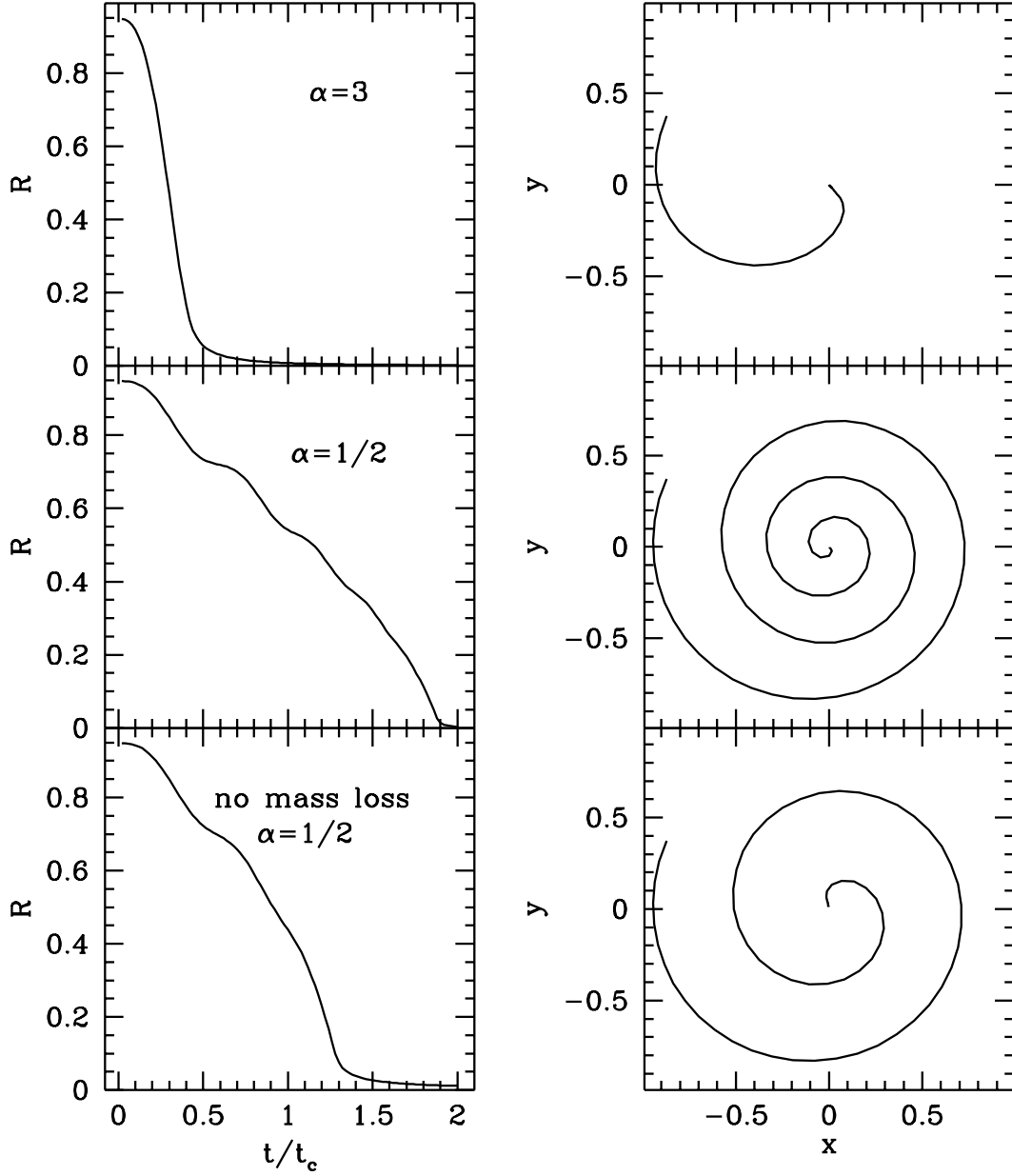


Figure 5. Orbits of satellites with various values of α . The stable clustering density profile of a CDM $10^{15}M_{\odot}$ was used to integrate the equations. The bottom panel shows an orbit if satellites did not lose mass as a result of tidal stripping.

3 RESULTS

We ran simulations with 80000 particles in the final halo and with 30000 equally-spaced time steps. In all the runs we set the softening parameter $\epsilon = 0.0005 r_v$, where r_v is the virial radius of the halo at the final time. For convenience we adjust the numerical factors in the equation such that α is the ratio of the dynamical friction time to the circular orbit time when the satellite just joined the halo. Following each time step, the satellites' lost energy is reassigned to particles in the halo.

It is interesting to inspect the effects of dynamical friction and tidal stripping. In figure 5, we plot trajectories of satellites moving in a halo with a density profile given by that of a $10^{15}M_{\odot}$ CDM halo as obtained assuming stable clustering and shown in Fig. 2. The satellites were initially placed on circular orbits in the XY plane. The orbits were integrated with $\alpha = 3$ and $1/2$ respectively. For comparison a trajectory with no tidal stripping is also shown.

Table 1. Slopes of density profiles in the region $10^{-2} < r/r_v < 10^{-1}$. For power law power spectra, M_1, M_2 and M_3 correspond to halos of masses 0.1, 1 and 10 in units of M_* . For CDM, they correspond to $10^{11}, 10^{13}$ and $10^{15}M_\odot$. Top and bottom values in each mass row are for the stable clustering and the semi-analytic dynamical model, respectively.

	$n = -2$	$n = -1$	$n = 0$	CDM
M_1	-1.45 -1.94	-1.84 -2.04	-2.12 -1.94	-1.59 -2.01
M_2	-1.38 -1.76	-1.65 -2.03	-1.90 -2.05	-1.41 -1.91
M_3	-1.26 -1.60	-1.54 -1.77	-1.76 -1.84	-1.25 -1.45

Fig. 6 shows density profiles of halos at the final time. Results are shown for halos with $M/M_* = 0.1, 1$ and 10 for the scale free power spectra and $M = 10^{11}, 10^{13}$ and $10^{15}M_\odot$ for the standard CDM model. The dotted lines show the best fit NFW profiles. The curves were computed assuming the satellites' lost energy was redistributed in the form of kinetic energy. The profiles in Fig. 6 were computed assuming $\alpha_{\max} = 1/2$. For the CDM model, the fraction of the total energy lost by satellites for this value of α_{\max} was 0.23, 0.11 and 0.04, for halos of mass $10^{11}, 10^{13}$ and $10^{15}M_\odot$, respectively. Fig. 7 shows the circular velocity profiles corresponding to the density profiles shown in Fig. 6.

Relative to the profiles obtained assuming stable clustering, these density profiles are steeper, at least in the inner regions. This is because the halo is heated by the infalling satellites. Recall that, in our prescription, energy lost by the satellites produces random motions among the halo particles. If the density profile is shallower than r^{-2} , then the number of particles crossing a radius r inward, as a result of the added random motions, is larger than the number of particles crossing outward. We have tried various other heating recipes such as redistributing only half the lost energy in the form of kinetic energy while the other half in the form of potential energy (by appropriately rescaling the radii of the halo particles). The final profiles in all the heating recipes we adopted were similar but not identical; they all were steeper than the corresponding profiles obtained from stable clustering.

Although the density profiles for $n > -2$, are not very well described by NFW fits, the density profiles for $n = -2$ and CDM are. The corresponding circular velocity profiles, plotted in Fig. 7, show significant deviations from the NFW fits. The slopes of the density profiles in the inner regions $r < 0.1r_v$ are listed in table 1. The top and bottom numbers in each row correspond to the profiles obtained from stable clustering (Fig. 2) and from the profiles in Fig. 6, respectively. It is interesting that the slope for the halo of mass $10^{15}M_\odot$ in the CDM model agrees with the result of the high resolution N-body simulation of Moore et. al. (1997).

4 SUMMARY AND CONCLUSIONS

Assuming gaussian initial conditions, we addressed two related issues. These were: *a*) how to generate random realisations of the growth history of a halo whose mass at the present time is given, and *b*) how the density profile of a halo can be related to its merging history.

The way we generate random realisations of halo histories is, in principle, different from that previously presented in the literature. Lacey & Cole (1993) and Eisenstein and Loeb (1996) choose to work with the function $f(M_1, z_1|M_0, z_0)$ which is the probability that a mass element of halo M_0 at z_0 is incorporated in a halo of mass M_1 at $z_1 > z_0$. Instead, we work with $N(M_1, z_1|M_0, z_0) = (M_0/M_1)f(M_1, z_1|M_0, z_0)$, which can be interpreted as the average number of progenitors of M_0 that have mass (M_1) at z_1 . We have checked that these previous methods lead to results that are similar to ours, and we show in the Appendix why this is so.

Given the mass growth rate we presented results using two models for computing the evolved density profiles. The first was based on the stable clustering assumption in which a mass element is effectively assumed to remain at the virial radius when it joined the halo. The second invoked a more detailed description of the motion of satellites once they have crossed the virial radius of the halo, incorporating tidal stripping, dynamical friction and heating of halo particles by infalling satellites. We found that including these effects leads to steeper profiles in the inner regions than in the stable clustering case. For initial power-spectra $P(k) \propto k^n$, we find that the slope in the inner regions depends on n , and also on the final mass. Table 1 shows that the inner profile is $\rho \propto r^{-\beta}$, with $\beta_{\text{SW}} \leq \beta \leq \beta_{\text{HS}}$. For a given power spectrum, the dependence of density profiles on the halo mass in our models is stronger than that seen in the simulations (e.g. NFW). In particular, for the CDM power spectrum, the relative difference between the profiles of halos of masses $10^{11}M_\odot$ and $10^{15}M_\odot$ is about an order of magnitude at $r = 0.1r_v$. On the other hand, the corresponding profiles in the simulations almost coincide for $0.1 < r/r_v < 1$. This suggests

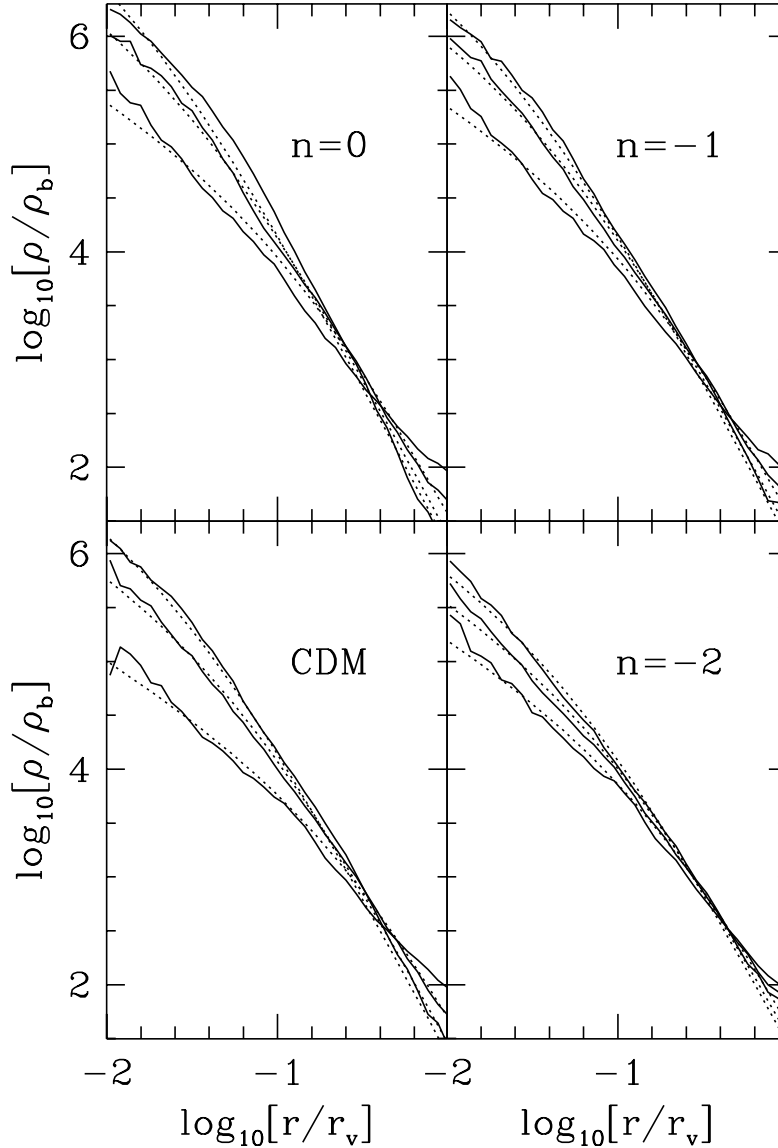


Figure 6. Density profiles obtained from the dynamical model using curves of $M(z)$ from Fig. 2. The dotted curves show the best NFW fits.

that the NFW argument that the concentration parameter is entirely determined by the formation time is inadequate. It is likely that effects, in addition to those included in our models, must play a significant role in determining halo density profiles. For example, in their study of fully three-dimensional collapse, Huss et al. (1998) suggest that a bar-related instability may play a major role in determining the final profile.

Using our simplified models, we hoped to shed some light on the current—arguably contradictory—results of various recent N-body simulations (Navarro Frenk & White 1997, Kravtsov et. al. 1997, Moore et. al. 1997) of halo density profiles. Based on these models, the general conclusion is that a one parameter form, such as the fit proposed by Navarro, Frenk & White (1997), is inadequate to describe the profiles for all radii and all power spectra.

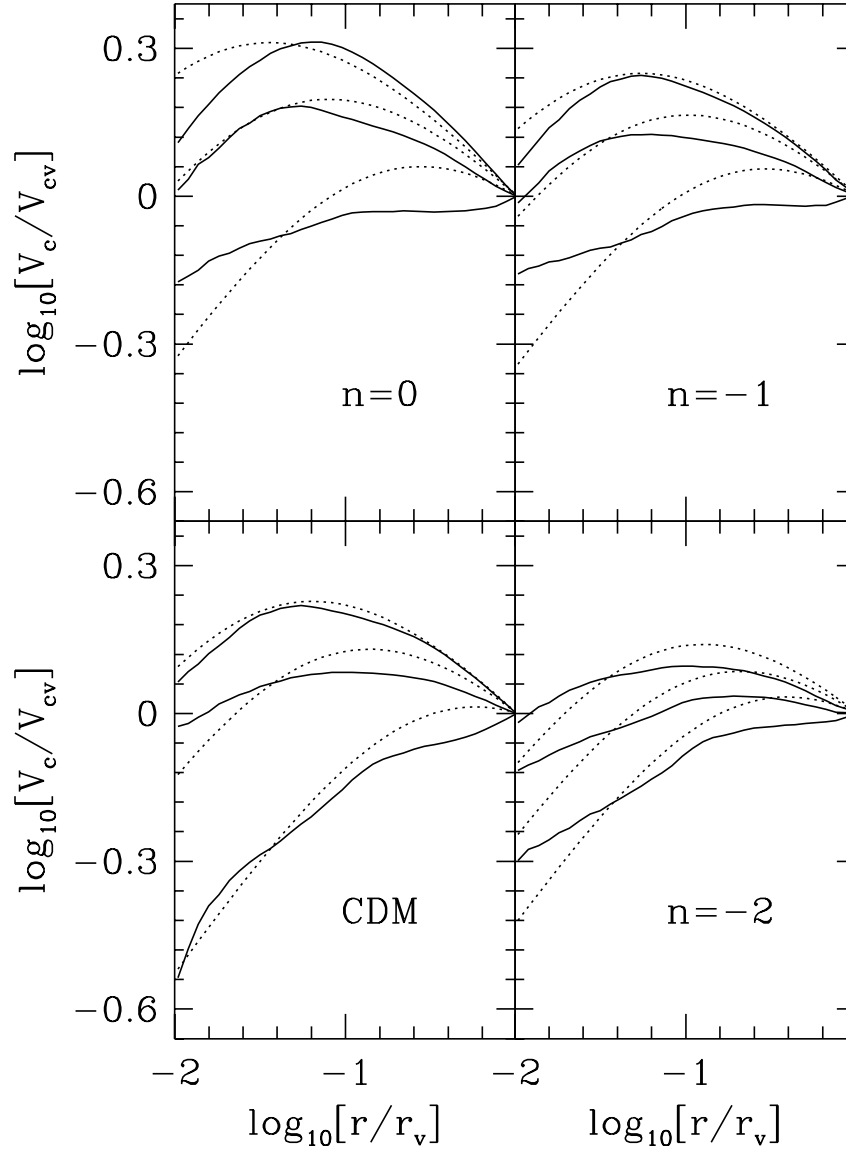


Figure 7. The same as the previous figure but showing circular velocity profiles.

ACKNOWLEDGMENTS

We thank Simon White, David Syer and Gerard Lemson for many useful discussions.

REFERENCES

- Avila-Reese V., Firmani C., Hernández X. 1997, astro-ph/9710201
 Bertschinger, E. 1985, *Astrophys. J. (suppl.)* 58, 39
 Bond, J.R., Kaiser, N., Cole, S. & Efstathiou, G. 1991, *Astrophys. J.* 379, 440
 Bower, R.G. 1991, *M.N.R.A.S.* 248,332

- Chandrasekhar, S. 1943, *Astrophys. J.* 97, 255
 Dekel, A. 1981, *Astron. Astrophys.* 101, 79
 Dubinski, J & Calberg, R. 1991, *Astrophys. J.* 378, 496
 Eisenstein, D.J. & Loeb, A. 1996, *Astrophys. J.* 459, 432
 Filmore, J.A. & Goldreich, P. 1984, *Astrophys. J.* 281, 1
 Gunn, J. & Gott, J.R. 1972, *Astrophys. J.* 179,1
 Hoffman, Y. & Shaham, J. 1985, *Astrophys. J.* 297, 16
 Hoffman, Y. 1988, *Astrophys. J.* i328, 489
 Huss A., Jain B., Steinmetz M. 1998, astro-ph/9803117
 Landau, L.D. & Lifshitz, E.M. 1960, *Mechanics*, (course of theoretical physics; V.1), Pergamon Press
 Kravtsov, A.V., Klypin, A.A., Bullock, J.S. & Primack, J.R. 1997, astro-ph/9708176
 Lemson, G. 1995, PhD. thesis, RIJKSUNIVERSITEIT GRONINGEN
 Lynden-Bell, D. 1967, *M.N.R.A.S.* 136, 101
 Moore, B., Chigna, S., Governato, F., Lake, G., Quinn, T. & Stadel, J. 1997, astro-ph/9711259
 Navarro, J.F., Frenk, C.S. & White, S.D.M. 1996, *Astrophys. J.* 462, 563
 Nusser, A. & Dekel, A. 1992, *Astrophys. J.* 362, 14
 Ostriker, J.P. & Turner, E.L. 1979, *Astrophys. J.* 234, 785
 Peebles, P. J. E. 1989, *Astrophys. J. (Lett.)* 344, 53
 Sheth, R.K. 1996, *M.N.R.A.S.* 291, 1277
 Sheth, R.K. & Pitman, J. 1997, *M.N.R.A.S.* 289, 66
 Syer, D. & White, S.D.M. 1996, astro-ph/9611065
 White, S.D.M. 1976, *M.N.R.A.S.* 177, 717
 White S.D.M., Zaritsky D. 1992, *Astrophys. J.* 394,1
 White, S.D.M. 1983, *Astrophys. J.* 274,53
 White, S.D.M. 1996, astro-ph/9602021
 Zhao, H.S. 1996, *M.N.R.A.S.* 278, 488

APPENDIX A: THE ALGORITHM

This Appendix describes our MMP generating algorithm in detail. First we compare our algorithm with others that have been proposed in the literature. Then we show that, in at least one respect, it is able to reproduce results measured in numerical simulations of hierarchical clustering. This motivates further study: we show that, for our algorithm, the distribution of formation times and the distribution of formation masses can be computed analytically.

A1 Comparison with previous work

Recall that the MMP is followed through a succession of small timesteps. At each step, the mass decreases according to equation (2). This means that the mass of the MMP is never smaller than half the mass of the parent halo at the previous time step. It is hard to justify this assumption on general theoretical grounds (but see Sheth & Pitman 1997 for a self-consistent, binary split model of the merger tree described by Sheth 1996). Nevertheless, this assumption is in agreement with results from N-body simulations; Fig. 5 in Tormen et al. (1997) shows that the masses of the MMPs in their simulations do not decrease by more than a factor of two at each small time step.

Our algorithm differs slightly from an MMP generating algorithm that was suggested by Lacey & Cole (1993), and used by Eisenstein & Loeb (1996). They split the MMP according to $f(1|0) = (M_1/M_0) N(1|0)$, with no restriction on M_1/M_0 [recall that the integral of $f(1|0)$ over the range $0 \leq M_1/M_0 \leq 1$ equals unity as required], but they then choose the larger of the two pieces. This means that their MMP has mass M_1 with probability $(M_1/M_0) N(M_1|M_0) + (M_0 - M_1)/M_0 N(M_0 - M_1|M_0)$, and $M_1 \geq M_0/2$ always. In the limit $(z_1 - z_0) \rightarrow 0$, $N(M_1|M_0) \approx N(M_0 - M_1|M_0)$, for a large range of M_1 (cf. Fig. 7 in Sheth & Pitman 1997), so this is similar to using $N(1|0)$ for the split rule. The approximation of equality is good for white-noise initial conditions, but it becomes worse for power spectra with $n < 0$.

Let t_f denote the formation time, defined as the time when the mass m of the MMP is a fraction f of the halo at the present time. Provided $f = m/M_0 \geq 0.5$, this distribution can also be computed using the arguments presented in section 2.5.2 of Lacey & Cole (1993). For white noise initial conditions (initial power spectra with slope $n = 0$), this distribution can be computed analytically. If

$$\omega_f \equiv \delta_{c0}(z_1 - z_0) / \sqrt{\sigma_m^2 - \sigma_{M_0}^2},$$

then, provided $f \geq 0.5$,

$$p(\omega_f) = \left(\frac{1}{f} - 1\right) 2\omega_f \operatorname{erfc}\left(\frac{\omega_f}{\sqrt{2}}\right) + \left(2 - \frac{1}{f}\right) \sqrt{\frac{2}{\pi}} \exp\left(-\frac{\omega_f^2}{2}\right), \quad (n = 0). \quad (\text{A1})$$

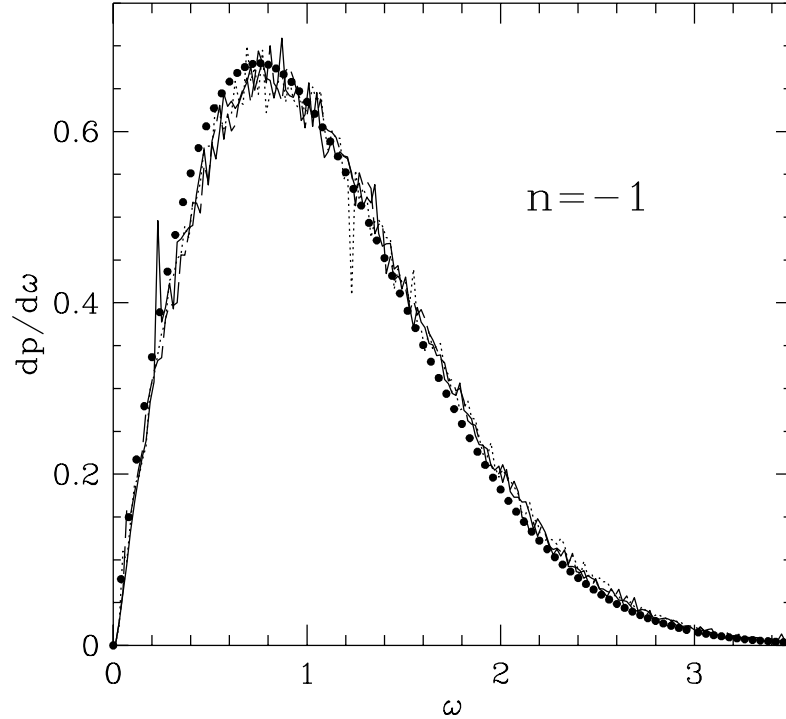


Figure A1. The distribution of the formation time of halos, expressed in terms of the variable $\omega = z(M_*/M)^{1/3}/\sqrt{(2^{2/3}-1)}$ for a power-law spectrum with slope $n = -1$. The dotted, solid and dashed curves correspond to $M/M_* = 0.1, 1$ and 10 , respectively. The points show equation (2.33) of Lacey & Cole (1993) for $n = 0$.

When $f = 0.5$ this reduces to equation (2.33) of Lacey & Cole (1993). For more general initial conditions the answer must be computed numerically. For all $f \geq 0.5$, the distribution for other values of n is very similar to that for $n = 0$ (Fig. 7 of Lacey & Cole 1993 shows this for $f = 0.5$). At least when $f = 0.5$, this distribution for the formation times fits the distribution measured in N-body simulations well (Lacey & Cole 1994). Since it is trivial to compute this distribution from our Monte-Carlo MMP generating algorithm (simply follow the MMP till its mass drops to f times the initial mass), it is important to check that our MMP generating algorithm is able to reproduce this distribution.

As a test of our MMP history scheme, Fig. A1 compares the distribution of formation times $p(t_f)$ obtained from our Monte-Carlo realizations with the analytic prediction given by (A1). The distributions are plotted in terms of the scaled variable ω_f , and we have set $f = 0.5$. Thus, $(t_0/t_f)^{2/3} = 1 + \omega\sqrt{2^\alpha - 1}(M_0/M_*)^{-\alpha/2}$ where $\alpha = (n+3)/3$ and n is the slope of the initial power spectrum. The figure shows results for $n = -1$, although our Monte-Carlo distributions for other values of n are also in good agreement with the analytic prediction, as are the distributions for other values of $f \geq 0.5$. The scatter of the Monte-Carlo distributions about the analytic prediction is also comparable to that seen in the N-body simulations. We use this fact to argue that our scheme provides MMP histories that are similar to those in the numerical simulations.

Fig. A1 shows the formation time distribution obtained directly from the numerical Monte-Carlo code. Since the distribution is in reasonable agreement with that found in N-body simulations, it may be worth studying our algorithm further. Below, we show how to derive explicit analytic expressions for the distribution of formation times and masses.

A2 Analytic calculation of the formation time distribution

Suppose a random variable Y is drawn from a Gaussian distribution with mean zero and variance χ . Then Y^2 has a $\text{Gamma}(\frac{1}{2}, \chi)$ distribution, and $X = Y^{-2}$ is said to have the $\text{Inverse Gamma}(\frac{1}{2}, \chi)$ distribution. That is,

$$p(X = x) dx = \frac{(\chi/x)^{1/2}}{\sqrt{2\pi}} \exp\left(-\frac{\chi}{2x}\right) \frac{dx}{x}. \quad (\text{A2})$$

Consider a sequence of random variables X_1, X_2, \dots , with each of the X_i s chosen from an $\text{Inverse Gamma}(\frac{1}{2}, \chi)$ distribution independently of the others. Define

$$S_n = \sum_{i=1}^n X_n. \quad (\text{A3})$$

It is easy to verify that the distribution of S_n is $\text{Inverse Gamma}(\frac{1}{2}, n^2\chi)$, so that

$$p_n(S_n = x) dx = \frac{(n^2\chi/x)^{1/2}}{\sqrt{2\pi}} \exp\left(-\frac{n^2\chi}{2x}\right) \frac{dx}{x}. \quad (\text{A4})$$

These expressions will be useful below.

Consider a halo that has mass M_0 at z_0 . Suppose that at $z_1 = z_0 + \Delta z$, the MMP of this halo has mass $0 \leq M_1 \leq M_0$ with probability $f(M_1, z_1|M_0, z_0)$, where $f(1|0)$ is given by equation (2). Note that, in the main text, we use a different function for the MMP probability. We use this form here to illustrate the way the calculation is done, and show the result of using our rule later. Then

$$(S_1 - S_0) = (\delta_{c0} \Delta z)^2 / y^2, \quad (\text{A5})$$

where y is drawn from a Gaussian distribution with zero mean and unit variance, so y^2 is drawn from a $\text{Gamma}(\frac{1}{2}, 1)$ distribution, which means that $1/y^2$ is drawn from an $\text{Inverse Gamma}(\frac{1}{2}, 1)$ distribution. Thus, the distribution of $(S_1 - S_0)$ is $\text{Inverse Gamma}(\frac{1}{2}, \chi)$, with $\chi = (\delta_{c0} \Delta z)^2$.

Suppose that, at $z_2 = z_1 + \Delta z$, the MMP of M_1 is obtained by drawing M_2 from $f(2|1)$, at $z_3 = z_2 + \Delta z$ the MMP of M_2 is drawn from $f(3|2)$, and so on. Then, after n steps,

$$(S_n - S_0) = (\delta_{c0} \Delta z)^2 \sum_{i=1}^n y^{-2}, \quad (\text{A6})$$

and the distribution of S_n is the distribution of the sum of n $\text{Inverse Gamma}(\frac{1}{2}, \chi)$ variates. Therefore, $p_n(S_n - S_0 = x) dx$ is given by equation (A4), with the obvious notation that

$$n^2\chi = n^2 (\delta_{c0} \Delta z)^2 = \delta_{c0}^2 (z_n - z_0)^2. \quad (\text{A7})$$

Define the formation time t_f as the first time that the mass of the MMP becomes less than fM_0 , with $0.5 \leq f \leq 1$. Let $S_f = \sigma^2(fM_0)$, and let z_f denote the redshift associated with the formation time. Suppose that Δz is chosen sufficiently small that $z_f - z_0 = n \Delta z$, with n an integer. Then, for this MMP generating rule, the formation time distribution is got from

$$\begin{aligned} P(t_f < t|M_0, t_0) &= P(S_n - S_0 < S_f - S_0) \\ &= \int_0^{S_f - S_0} p_n(x) dx \\ &= \text{erfc}\left(\frac{\delta_{c0}(z_f - z_0)}{\sqrt{2(S_f - S_0)}}\right). \end{aligned} \quad (\text{A8})$$

This is the same as equation (2.23) in Lacey & Cole (1993).

Suppose instead that the MMP is not chosen according to $f(1|0)$, but it is chosen using $N(1|0) = (M_0/M_1) f(1|0)$, with the requirement that $M_0/2 \leq M_1 \leq M_0$. This is the choice we make in the main text. (Recall that, as $\Delta z = (z_1 - z_0) \rightarrow 0$, the integral of $N(1|0) \rightarrow 1$.) Suppose further that at $z_2 = z_1 + \Delta z$ the MMP of M_1 is chosen from $N(2|1)$, with $M_1/2 \leq M_2 \leq M_1$. Then,

$$p(S_2) = \int_{S_{\min}}^{S_2} N(2|1) N(1|0) dS_1, \quad (\text{A9})$$

where $S_{\min} = S_0$ if $S_2 < S(M_0/2)$, and $S_{\min} = S(2M_2)$ otherwise. These restrictions on S_{\min} follow from the requirements that, in any step, the mass of the MMP may not decrease to less than half the current mass, and the mass of the MMP can never be greater than M_0 . Now, if $S_2 < S(M_0/2)$, then this is the same convolution integral as the split rule by $f(1|0)$ above, since the extra factors $(M_1/M_2)(M_0/M_1) = (M_0/M_2)$ may be taken outside the integral. Thus, provided that $M_2 \geq M_0/2$,

$$p(S_2) = \left(\frac{M_0}{M_2}\right) f(2|0) = N(2|0). \quad (\text{A10})$$

Choose some $0.5 \leq f \leq 1$. If $M_i \geq M_0/2$ for $1 \leq i \leq n$, then after n steps, $p(S_n) = N(S_n|S_0)$, and

$$P(t_f < t|M_0, t_0) = \int_{fM_0}^{M_0} N(m, z_f|M_0, z_0) dm, \quad (\text{A11})$$

where $z_f - z_0 = n \Delta z$ as before. This expression is the same as equation (2.26) in Lacey & Cole (1993). This demonstrates that, for sufficiently small steps in Δz , choosing the MMP using $N(1|0)$ of equation (2) gives the correct distribution of formation times (equation A1).

A3 Analytic calculation of the distribution of formation masses

Suppose that the formation time is defined as above for some $0.5 \leq f \leq 1$. Then the formation mass M_f may be defined in at least two ways. The first is to define it as the smallest mass M for which $M > fM_0$, averaged over all merger histories. This is the same definition as that shown in Figure 11 of Lacey & Cole (1993). Alternatively, we could define the formation mass as the largest mass M at which $M < fM_0$, averaged over all histories. Compared to the quantity in the first definition, this is the mass of the MMP in the next time step. For either definition, in the appropriate units, the distribution of formation masses for a white-noise spectrum (initial slope $n = 0$) provides an excellent fit to the distribution for other power spectra. (Recall that the same is true for the formation time distribution.) This is fortunate, since, when $n = 0$, then, for our MMP generating algorithm, the distribution of formation masses can be calculated analytically. We show this below.

As above, it is convenient to work in terms of the variable S rather than M . The quantity described by the first definition can be computed as follows. The probability that $M_f = M$ is equal to the probability that after step n the mass was $M_n = M > fM_0$, and that the mass dropped to $M_{n+1} < fM_0$ on step $n + 1$, integrated over all allowed values of M_{n+1} , and summed over all values of n . The sum over all n allows for all possible formation times. Thus,

$$\begin{aligned} p(M) dM &= p(S) dS \\ &= dS \sum_{\text{allowed } n} \int_{S_f}^{S(M/2)} p(S_{n+1}|S_n = S) p(S_n = S|S_0) dS_{n+1}, \end{aligned} \quad (\text{A12})$$

where $S_f = S(fM_0)$. The upper and lower limits to the integral reflect the fact that the allowed values of M_{n+1} are all those that are smaller than fM_0 but larger than $M_n/2$. Now, the order of the sum and the integral can be rearranged. Since $p(S_{n+1}|S_n = S)$ is just the one-step split rule, it is independent of n , so it is convenient to do the sum over n first. Since S_n is less than $S_f = S(fM_0)$, the previous section showed that, for our algorithm, $p(S_n|S_0) dS_n = N(S_n, z_n|S_0, z_0)$. Moreover, for small Δz , summing over n is like integrating over all formation times z_f . Thus,

$$\begin{aligned} dS \sum_n p(S|S_0) &\rightarrow \frac{dS}{\Delta z} \int_0^\infty dz_f N(S, z_f|S_0, z_0) \\ &= \frac{dS}{(S - S_0)} \frac{(M_0/M)}{\Delta z} \sqrt{\frac{S - S_0}{2\pi\delta_{c0}^2}}. \end{aligned} \quad (\text{A13})$$

This expression is independent of M_{n+1} . For a white-noise power-spectrum, $M/M_{n+1} = S_{n+1}/S$, so the integral over the allowed range of S_{n+1} can be done analytically:

$$\int_{S_f}^{S(M/2)} N(S_{n+1}|S_n = S) dS_{n+1} = 2\sqrt{\frac{D}{\pi}} \left(e^{-D} - \frac{e^{-Dq}}{\sqrt{q}} \right) + (1 - 2D) \left(\text{erf}(\sqrt{Dq}) - \text{erf}(\sqrt{D}) \right) \quad (\text{A14})$$

where $D = (\delta_{c0} \Delta z)^2 / 2S$, and $q = S/(S_f - S)$. Thus, as $\Delta z \rightarrow 0$, so $D \rightarrow 0$, then, provided $Dq \ll 1$,

$$p(s) ds \rightarrow \frac{1}{m\pi} \frac{ds}{\sqrt{(s-1)(s_f-s)}} \left(2 - \frac{s_f}{s} \right), \quad \text{for } n = 0, \quad (\text{A15})$$

where $s = S/S_0$, $s_f = S_f/S_0$, and $m = M/M_0$. In this limit, the dependence on Δz has dropped out.

The quantity described by the second definition can be computed similarly. The probability that $M_f = M$ is equal to the probability that after step n the mass was $M_n > fM_0$, and that the mass dropped to $M < fM_0$ on step $n + 1$, integrated over all allowed values of M_n , and summed over all choices of n . That is,

$$\begin{aligned} p(M) dM &= p(S) dS \\ &= dS \sum_{\text{allowed } n} \int_{S_{\min}}^{S_f} p(S_{n+1} = S|S_n) p(S_n) dS_n, \end{aligned} \quad (\text{A16})$$

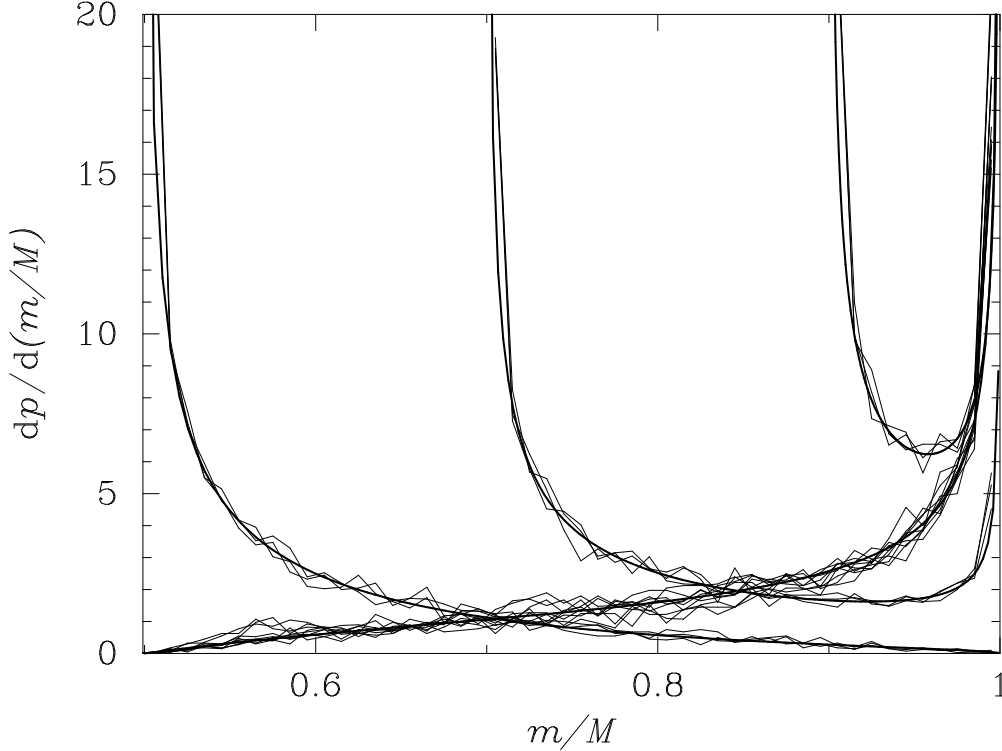


Figure A2. Distribution of formation masses using our MMP generating algorithm. The thick solid curve that is lowest on the left shows equation (A19) with $f = 0.5$ and $M = fM_0$. Curves for other values of f are similar so we have not shown them. The other thick curves show equation (A15) with $f = 0.5, 0.7$ and 0.9 , and $M = M_0$. The thin curves show the corresponding quantities computed using our Monte-Carlo algorithm for a range of values for the spectral slope n ($0, -1$ and -2), the final mass M_0 ($0.1, 1$, and $10M_*$), and the time step Δz (0.01 - 0.1). All the curves are very similar, and they are well fit by the analytic (white-noise) formulae.

where $S_{\min} = S(2M)$ if $2M < M_0$, and $S_{\min} = S_0$ otherwise because, for our algorithm, $M_f = M$ must lie in the range $fM_0/2 \leq M \leq fM_0$. This means that M_n lies in the range $M \leq M_n \leq 2M$, unless $2M > M_0$, in which case the maximum allowed value of M_n is simply M_0 . The sum is over all formation times, so it is over all $n > 0$. Now, as before, $p(S_n) dS_n = N(S_n, z_n | S_0, z_0)$, and $p(S_{n+1} = S | S_n)$ is just the one step split rule, so it is independent of n . If we rearrange the order of the sum and the integral above, then, for small Δz , summing over n is like integrating over all formation times z_f , so the integral is the same as before:

$$\begin{aligned} dS_n \sum_n p(S_n) &\rightarrow \frac{dS_n}{\Delta z} \int_0^\infty dz_f N(S_n, z_f | S_0, z_0) \\ &= \frac{dS_n}{(S_n - S_0)} \frac{(M_0/M_n)}{\Delta z} \sqrt{\frac{S_n - S_0}{2\pi\delta_{c0}^2}}. \end{aligned} \quad (\text{A17})$$

Using this expression and then doing the integral over the allowed range of S_n implies that

$$p(S) dS = \frac{dS}{S - S_0} \left(\frac{M_0}{M}\right) \frac{e^{-A}}{\sqrt{A}} [\text{erf}(\sqrt{AB}) - \text{erf}(\sqrt{AC})] \quad (\text{A18})$$

where

$$A = \frac{(\delta_{c0} \Delta z)^2}{2(S - S_0)}, \quad B = \left(\frac{S_f - S_0}{S - S_f}\right), \quad \text{and } C = \max\left(0, 1 - \frac{S_0}{S_{\min}}\right).$$

For small Δz , the error function terms become $2\sqrt{(A/\pi)}(\sqrt{B} - \sqrt{C})$ provided $(S - S_f)/S_f$ is not small. In this approximation, the formation mass distribution is

$$\begin{aligned} p(s) ds &= \left(\frac{M_0}{M}\right) \frac{1}{\pi(s - s_0)} \sqrt{\frac{1 - s_0}{s - 1}} ds && \text{if } 2M > M_0, \\ &= \left(\frac{M_0}{M}\right) \frac{1}{\pi(s - s_0)} \left[\sqrt{\frac{1 - s_0}{s - 1}} - \sqrt{1 - \frac{s_0}{s_{\min}}} \right] ds && \text{if } M_0 \geq 2M \geq fM_0, \end{aligned} \quad (\text{A19})$$

where $s_i \equiv S_i/S_f$. Notice that, in this limit, the dependence on Δz has dropped out.

As with the distribution of formation times, this is a well-behaved probability distribution only for white-noise, where $s_i = S_i/S_f = fM_0/M_i$. However, as with the formation time distribution, this distribution depends only very weakly on power spectrum, so the white-noise expression provides a good fit to the distribution for other power-spectra. It also turns out that this distribution depends only weakly on f , so, in Figure A2, only the curve for $f = 0.5$ is shown.

Figure A2 shows both formation mass distributions for a range of initial power-spectra, final M_0 s, and choices for f . The x -axis shows M_f/M_0 for equation (A15), and $M_f/(fM_0)$ for equation (A18). The thick solid curves show the analytic formulae with $f = 0.5, 0.7$ and 0.9 , for $M/M_* = 0.1, 1$, and 10 , and $n = 0$. The thinner lines show the associated distributions obtained using our MMP generating code for $n = 0$ (solid), $n = -1$ (dashed), and $n = -2$ (dotted). The curves for the different power-spectra are virtually indistinguishable, and they are all well fit by our analytical formulae. This, and the fact that our code also generates the correct distribution of formation times (Fig. 1), shows that our MMP generating code works.